Desalination and Water Treatment
www.deswater.com
doi: 10.5004/dwt.2022.28912

274 (2022) 39–48
October

Hybrid cellulose nanocrystals and graphene oxide polysulfone membranes for copper removal

Siti Nurul Najiah A. Rasid[a], Nor Azura C. Mahmud[a], Syed M. Saufi[a,*], Mohd Sobri Takriff[b,c], Wei Lun Ang[b]

[a]*Department of Chemical Engineering, College of Engineering, Universiti Malaysia Pahang, Lebuhraya Tun Razak, 26300 Gambang, Kuantan, Pahang, Malaysia, emails: smsaufi@ump.edu.my (S.M. Saufi), najiahrasid95@gmail.com (S.N.N.A. Rasid), norazuraa123@gmail.com (N.A.C. Mahmud)*
[b]*Department of Chemical and Process Engineering, Faculty of Engineering and Built Environment, Universiti Kebangsaan Malaysia, 43600 Bangi, Selangor, Malaysia, emails: mtakriff@sharjah.ac.ae (M.S. Takriff), wl_ang@ukm.edu.my (W.L. Ang)*
[c]*Chemical and Water Desalination Engineering Program, College of Engineering, University of Sharjah, United Arab Emirates*

Received 1 March 2022; Accepted 4 September 2022

ABSTRACT

Polysulfone (PSF) membranes blended with cellulose nanocrystals (CNC) and graphene oxide (GO) nanofiller were prepared for copper removal in this study. The impacts of single CNC, GO, and mixed CNC-GO addition on the morphology, hydrophilicity, permeability, copper ion rejection, and membrane binding capacity were discussed. Scanning electron microscopy results showed that incorporating CNC, GO, and CNC-GO resulted in a more porous membrane structure with a high porosity value. The hydrophilicity of hybrid CNC-GO-PSF membranes were improved with the increment of CNC content and inclusion of the GO filler. Hybrid membranes showed a significant increment of flux compared to pristine PSF membrane. The water flux of the hybrid P-1GO-2C membrane is 8-fold higher than the pure PSF membrane (3.31 L/m^2·h). However, the copper rejection of the hybrid CNC-GO-PSF membranes was less than 50%. The increment of the CNC in the hybrid CNC-GO-PSF membrane increases the membrane porosity, and the sub-layer structure of the membrane is becoming very loose. In adsorptive filtration mode, the GO-PSF membrane showed the highest copper binding capacity of 8.49 mg·Cu/g membrane.

Keywords: Cellulose nanocrystal; Hybrid membrane; Copper removal; Graphene oxide; Water treatment

1. Introduction

Contamination of heavy metals in water has become a severe problem due to the rapid growth of modern manufacturing. Toxic heavy metals such as cadmium, lead, chromium, mercury, arsenic, and copper have been reported to pose a risky impact on public health and biosystems [1]. It has also been identified as a high-risk threat to terrestrial animals and aquatic life cycles [2]. Among them, copper at higher concentrations beyond a permissible limit is carcinogenic and mutagenic. It is very toxic to living organisms and is considered a possible agent that causes cancer [3]. According to the Malaysian Emission Standards, the maximum concentration limit of Cu(II) should be below 1.0 mg/L [4,5]. Copper removal in our everyday water usage has become an essential concern because it is one of the most commonly used metals in the electroplating, storage, and mining industries [6]. Appropriate handling and treatment for removing copper to below the standard levels have thus become a common goal for many researchers.

Membrane technology has emerged as a revolutionary process in water purification and heavy metals removal

* Corresponding author.

from wastewater effluent. The membrane process's advantages are no phase change operation, acceptable energy consumption, and better efficiency compared to other techniques [7,8]. Ultrafiltration (UF) membranes, which have been primarily developed and commercialized over the last three decades, are the desired membrane for this purpose due to the low-pressure operation requirement. Polysulfone (PSF)-based membranes have been used as high-performance UF membranes in many applications nowadays. For instance, a highly permeable PSF membrane with high selectivity for copper removal was produced by blending PSF with clay and zeolite [4,9]. Mondal and Kumar Majumder [10] prepared a series of PSF composite UF membranes for adsorptive removal of heavy metals such as Pb^{2+}, Cu^{2+}, Cd^{2+}, and Fe^{2+} from aqueous solutions. Moradihamedani and Abdullah [11] had blended PSF with cellulose acetate to produce a UF membrane capable of rejecting 98% of Pb^{2+}.

Recently, nanomaterials have been widely employed in many water treatment studies with promising outcomes, significantly improving the overall treatment efficiency and water quality [12]. In this context, nanomaterial with high reactivity, high surface area, unique morphologies, and functionality can be adopted and used as an additive in the membrane matrix. In an attempt to achieve sustainable materials, nanocellulose-based materials that are the most abundant biopolymer on Earth have drawn the attention of membrane researchers. Cellulose nanocrystal (CNCs) have gained significant interest as nanofillers in polymer composites due to their abundant functional groups, high mechanical properties, large surface area, renewability, low cost, and biodegradability [13–15]. The incorporation of CNC in polymer increased the mechanical strength of the polymeric membrane [16]. The surface of the CNC is also abundant in hydroxyl groups [17] which can be integrated with several chemical functionalities to adsorb various pollutants in water, such as bacteria, viruses, dyes, and heavy metals [12,18]. The use of CNC in thin-film composite membranes, where complexation enabled by the membrane's abundant hydroxyl and amine groups, resulted in a boron rejection rate approaching 90% [19]. Besides, the hydroxyl group on the CNC surface could enhance the hydrophilicity and antifouling properties of the polymeric membranes [20]. The addition of a hydrophilic CNC to the active layer of the PA membrane resulted in a 1.6-fold increase in pure water flux due to the increased membrane hydrophilicity [21].

Other important nanomaterials involved in membrane synthesis are carbon-based materials such as carbon nanotubes, graphene, and graphene oxide (GO). Carbon-based materials have a strong mechanical ability, high tolerance to strong acids/alkaline and organic solvents, and simple usability [22]. GO was seen as one of the emerging nano-building materials to fabricate novel separation membranes due to its distinct two-dimensional (2D) and single-atom-thick structure, high mechanical strength, and high chemical inertness [23]. GO contains many oxygenated functional groups, such as hydroxyl, epoxy, and carboxyl, which provide GO with high hydrophilicity and favourable water solubility [24,25]. The incorporation of GO into the membrane had improved membrane porosity, flux, hydrophilicity, and mechanical properties [26–28]. A stable PSF-GO mixed matrix membrane with >90% of Cr(VI), Cu(II), Pb(II), and Cd(II) removal efficiency was prepared by Mukherjee et al. [29]. By introducing GO, the membrane's permeability increases due to non-solvent de-mixing, resulting in a spongy membrane matrix that contributes to the membrane's increased permeability. In addition, a large number of oxygen atoms on the GO surface provided a lone pair of electrons that can bind with the heavy metal effectively [10].

The incorporation of CNC and GO (separately) in the synthesis of UF membranes has improved the properties of membranes, which benefit the removal of pollutants. However, the mixed incorporation of CNC and GO in the same membrane was not extensively investigated. Recently, Zhang et al. [30] prepared a hybrid membrane by attaching GO to the surface of the CNC functionalized poly(vinylidene fluoride) membrane to filter micro-polluted water. It is anticipated that the incorporation of both materials in the membrane could give synergistic benefits in water filtration. Therefore, the feasibility of blending CNC and GO in the same PSF membrane matrix for copper removal was investigated in this study. The hybrid membrane was tested for normal and adsorptive filtration modes to evaluate copper rejection and adsorption capacity, respectively.

2. Experiments

2.1. Materials

All the chemicals were analytical grade and used as received without purification. Microcrystalline cellulose (MCC) was purchased from R&M Chemicals (Malaysia), Low Dimensional Materials Research Centre, University of Malaya, Malaysia supplied GO, and PSF was from Radel® A, Solvay (USA). Copper standard solution, N-methyl-2-pyrrolidone (NMP), and sulfuric acid (H_2SO_4) were purchased from Merck (Malaysia). Deionized (DI) and ultrapure water were used for membrane preparation and characterization.

2.2. Procedure of CNC preparation

CNC suspension was prepared from MCC by acid hydrolysis using sulfuric acid [31]. MCC of 5 g was mixed with 50 mL of sulfuric acid aqueous solution (64 wt.%), and the mixture was vigorously stirred at 40°C for 2 h. The suspension was immediately diluted five times with DI water to stop the hydrolysis reaction. Subsequently, the suspension was centrifuged at 4,500 rpm for 10 min to precipitate the CNC from the suspension and eliminate excess aqueous acid. The washing and centrifugation steps were repeated several times before being dialyzed using a cellulose membrane dialysis tube (MWCO 14000) against DI water for several days. The dialyzed suspension was then sonicated for 10 min to re-disperse the solid aggregates in the suspension at 5°C and freeze-dried to create a stable CNC powder.

2.3. Membrane preparation

PSF bead was dissolved in NMP to produce PSF polymer solution with 15 wt.% of polymer concentrations. CNC and GO powders with different ratios (Table 1) were added to the polymer solution. The solution was stirred continuously for approximately 4–6 h at 60°C. The solution

Table 1
Formulation of hybrid CNC-GO-PSF membrane based on 100 g dope solution

Membrane	PSF (wt.%)	CNC (wt.%)	GO (wt.%)	NMP (wt.%)	Total (g)
P	15	–	–	85	100
P-1GO	15	–	1	84	100
P-1C	15	1	–	84	100
P-1GO-0.5C	15	0.5	1	83.5	100
P-1GO-1C	15	1	1	83	100
P-1GO-1.5C	15	1.5	1	82.5	100
P-1GO-2C	15	2	1	82	100

was left for several hours at room temperature to remove air bubbles. A casting machine was used to cast the dope solution onto a glass plate with adjusted thickness to 100–120 μm. The film was immersed in water as a coagulation medium for 1 h, and subsequently, it was left in a large amount of water for another 24 h. Then, the film was dried in an open-air for 1 d.

2.4. Morphology analysis

The cross-sectional morphologies of membranes were examined using a scanning electron microscopy (SEM) analysis (Philips SEM/EDAX; XL-40; PW682/10, The Netherlands) with a 20.0 kV potential. Membranes were immersed in liquid nitrogen and mounted vertically on carbon tape for cross-sectional analysis. Before the SEM analysis, membranes were vacuum coated with a thin layer of gold.

2.5. Porosity analysis

The porosity of membranes was estimated using dry-wet weight methods [32]. The membrane pieces were soaked in DI water at room temperature for 24 h. Wet membrane pieces were immediately evacuated, carefully cleaned using dry filter paper to eliminate excess water droplets, and weighed. The membrane was then dried in a 60°C oven for another 24 h before being weighed again. Eq. (1) was used to calculate the membrane's overall porosity.

$$\text{Porosity} = \frac{\left(w_1 - w_2\right)}{\rho v} \times 100\% \tag{1}$$

where w_1 and w_2 are the mass of membrane in wet and dry states (mg), respectively. ϱ is the density of water (mL/mg), and v is the membrane volume in the wet state (cm^3).

2.6. Static water contact angle analysis

5 μL of water was dropped on the membrane surface using stainless steel needle syringe. Membrane contact angles were determined using a contact angle goniometer (CAM 101 Optical Contact Angle Meter, KSV Instruments, China). The average contact angle was reported based on three different membrane locations of the same membrane sample.

2.7. Pure water flux and permeability measurement

The pure water flux, J_w (L/m^2·h), and pure water permeability (PWP) (L/m^2·h·bar) of the membranes were measured using 300 mL Sterlitech HP4750 (Sterlitech Corporation, USA) dead-end filtration system. Firstly, the membrane sample (14.6 cm^2) was pressurized at 5 bar to steady flux for 2 h. The permeation experiment was performed at three different pressures (3, 2, and 1 bar) for 1 h. The permeate flux and PWP were calculated using Eqs. (2) and (3), respectively:

$$J_w = \frac{v}{A_m \Delta T} \tag{2}$$

$$\text{PWP} = \frac{J_w}{\Delta P} \tag{3}$$

where J_w is the permeation flux of the (L/m^2·h), v is the volume of permeate (L), A_m is the effective area of the membrane (m^2), ΔT is the permeation time (h), PWP is pure water permeability, and ΔP is pressure difference (bar).

2.8. Copper filtration and binding experiment

The setup for the copper filtration experiment was similar to the pure water flux measurement. The filtration was performed at 3 bar using 50 mg/L copper ion solution as the feed solution. The copper concentrations in the permeate sample were measured using atomic absorption spectroscopy to calculate the rejection using Eq. (4).

$$\text{Rejection}\left(\%\right) = \left(1 - \frac{C_p}{C_f}\right) \times 100 \tag{4}$$

where C_p and C_f are the concentration of copper ion (mg/L) in permeate and feed, respectively.

After the filtration, the copper content in the retentate and permeate was analysed to calculate the copper binding capacity in adsorptive filtration mode. Mass balance was performed to estimate the copper adsorbs on the membrane. The adsorption capacity was computed based on the amount of copper adsorb per mass of the membrane used, as shown in Eq. (5).

$$\text{Binding Capacity}\left(\text{mg Cu/g membrane}\right) = \frac{V_f C_f - V_p C_p - V_r C_r}{m} \tag{5}$$

where C_f, $C_{p,}$ and C_r are the copper ion concentrations in the feed, permeate, and retentate, respectively. V_f, $V_{p,}$ and V_r are the volume of feed, permeate, and retentate, respectively, and m is the mass of the membrane used.

3. Results and discussion

3.1. Morphology of membranes

The full SEM cross-sectional images of PSF membranes at different compositions of CNC and GO are presented in

Fig. 1 at 2,000× magnification. SEM images show that all the prepared membranes have a dense top layer and a porous sub-layer, which is the typical asymmetrical structure of the UF membrane. A different form of porous sub-layer can be observed. P-1GO membrane showed large macro voids near the bottom part of the membrane. The large macro voids are formed when the mass transfer rate between the solvent and the non-solvent increases during the phase inversion process. As the GO has strong hydrophilicity characteristics, it enhanced this solvent-non-solvent mass transfer rate during the membrane formation [33,34]. Pristine PSF and P-1C have a similar asymmetric membrane structure. The amount of the CNC in the hybrid CNC-GO-PSF membrane affects the bottom sub-layer part of the membrane accordingly. The size of the bottom macro voids increased as the amount of the CNC increased in the hybrid membrane. According to Lv et al. [35], the hydrophilic GO-CNC composites changed the thermodynamic instability of the casting solution. They accelerated the diffusion of non-solvent into the casting solution during the gelation process, speeding up the demixing rate and resulting in more and larger pore channels after solidification.

The upper portion of the membrane sub-layer also shows a different morphology, as shown by the SEM image in Fig. 2 captured at 10,000× magnification. Pristine PSF, P-1GO, and P-1C membranes showed a single layer of cylindrical pores membrane structure. Meanwhile the hybrid membrane containing GO and CNC showed two distinct forms of upper porous sub-layer. The first layer, below the membrane top layer, consists of microporous cylindrical pores. The second layer is the major sub-layer portion, which consists of large macro voids pores. Further addition of CNC in the hybrid CNC-GO-PSF membrane had reduced the portion of the microporous first sub-layer structure but increased the portion and size of the macro void of the second sub-layer accordingly. CNC and GO have high hydrophilicity,

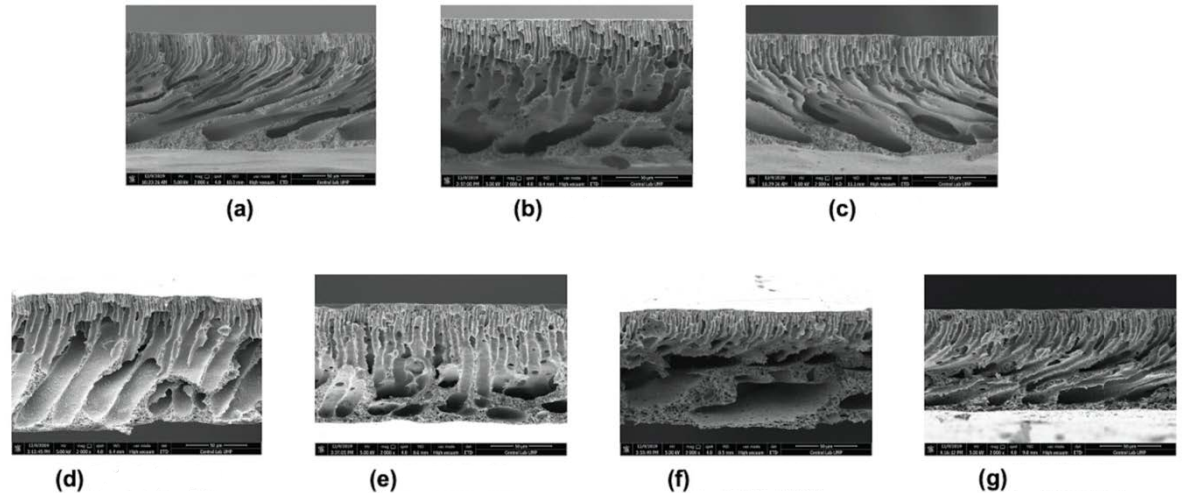

Fig. 1. Cross-sectional SEM images of the membranes at 2,000× magnification. (a) P, (b) P-1GO, (c) P-1C, (d) P-1GO-0.5C, (e) P-1GO-1C, (f) P-1GO-1.5C, and (g) P-1GO-2C.

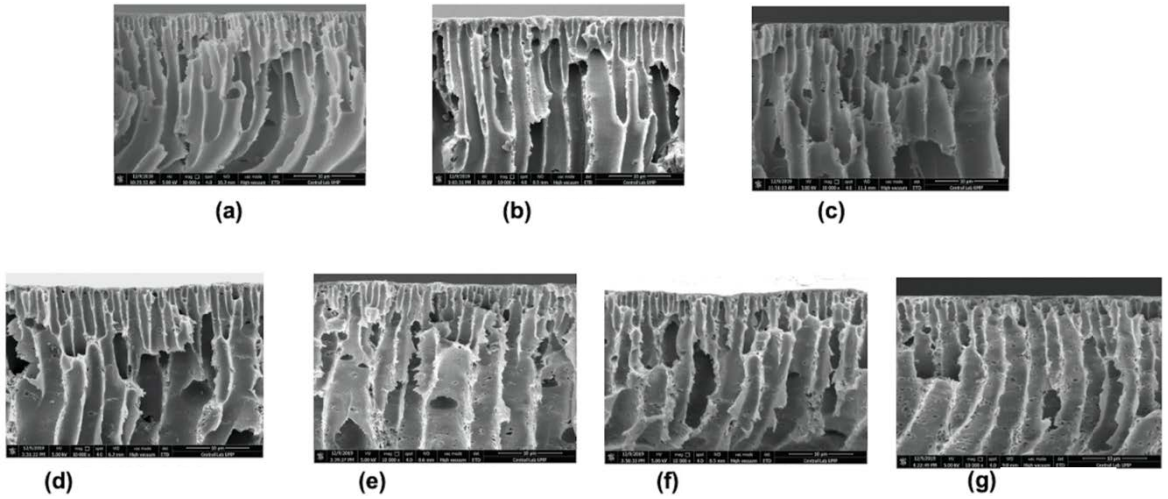

Fig. 2. Cross-sectional SEM images of the upper portion of membrane sub-layer at 10,000× magnification. (a) P, (b) P-1GO, (c) P-1C, (d) P-1GO-0.5C, (e) P-1GO-1C, (f) P-1GO-1.5C, and (g) P-1GO-2C.

which exchanges more water during the phase inversion [36], accelerates the mass transfer between the solvent and non-solvent, and results in a larger macro void sub-layer. The above results were consistent with the other reports [28,35].

Fig. 3 shows the SEM top surface of PSF and hybrid CNC-GO-PSF membranes. The GO and CNC fillers were wholly embedded and intercalated within the PSF matrix as no particulate material can be physically observed on the membrane surface. The pristine PSF membrane exhibits a smooth and flat surface. In contrast, the hybrid CNC-GO-PSF membrane exhibited rough surfaces with numerous pores. As the amount of CNC increased in the hybrid CNC-GO-PSF membrane, the size and number of pores were increased accordingly.

3.2. Porosity

The porosity of the membranes is represented in Fig. 4. Pristine PSF membrane showed the lowest porosity of 64.46% ± 7.35%. The P-1GO-2C membrane exhibits the highest porosity with 91.69% ± 2.05% porosity. Generally, the addition of CNC and GO to the PSF membrane enhanced the porosity of the membranes. CNCs are an excellent hydrophilic material with a high-water absorption ability. Hydrophilic nanoparticles help to form higher porosity and more extensive pore radius membranes during the phase inversion process [37]. Also, the hydrophilicity effect of GO expedited the exchange of solvent/non-solvent during the phase inversion process, which led to higher membrane porosity [27]. Similar findings were reported by Wang et al. [28] when polyvinylidene fluoride (PVDF) membranes were mixed with GO. The combination of GO with CNC in the hybrid CNC-GO-PSF membrane accelerated the diffusion rate of the solvent to the casting solution, which contributed to the formation and growth of the pores inside the membrane matrix.

3.3. Water contact angle

The contact angle is an essential measure of membrane surface hydrophilicity. The surface's hydrophilicity increased when the contact angle was reduced [37]. The effect of the CNC and GO content on membrane surface hydrophilicity in the casting solution is shown in Fig. 5. The pristine PSF membrane had a maximum contact angle of 98.8°, corresponding to the lowest hydrophilicity. Single nanofiller addition improved the membrane's hydrophilicity in P-1GO and P-1C membranes. P-1GO exhibited a water contact angle of 59, comparable to the PSF-GO (contact angle range of 53–65) membrane prepared by Ganesh et al. [26]. The contact angle of the P-1C membrane is 67, slightly lower when compared to the PSF-GO (contact angle range of 76–88) membrane produced by Yang et al. [20]. P-1GO membrane shows more hydrophilic than the P-1C membrane. According to Zinadini et al. [34], the hydrophilic GO migrates toward the top surface of the membrane as the top layer is more exposed to water (non-solvent) during the membrane formation. This migration decorates the functional groups of GO on the membrane top surface and improves the membrane hydrophilicity. In addition, the rough surface of the P-1C membrane (as can be seen in Fig. 3c) counteracted the hydrophilic effect of CNC when

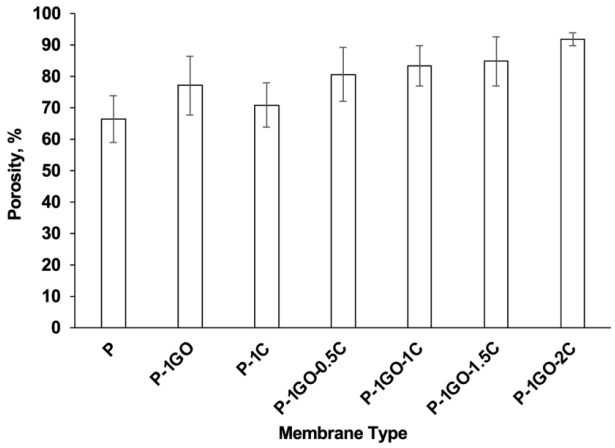

Fig. 4. Porosity of the membranes.

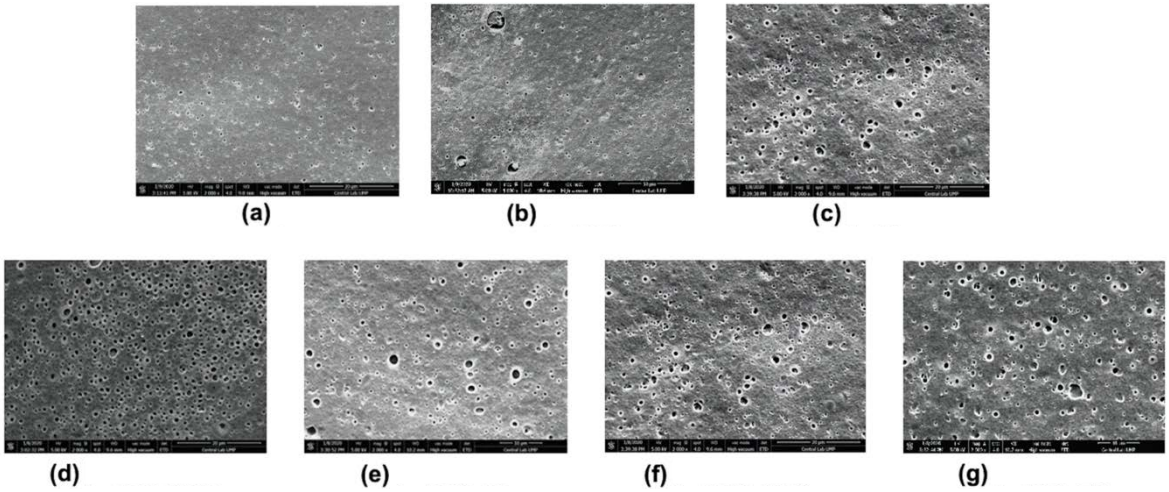

Fig. 3. Top surface SEM images of the membranes at 2,000× magnification. (a) P, (b) P-1GO, (c) P-1C, (d) P-1GO-0.5C, (e) P-1GO-1C, (f) P-1GO-1.5C, and (g) P-1GO-2C.

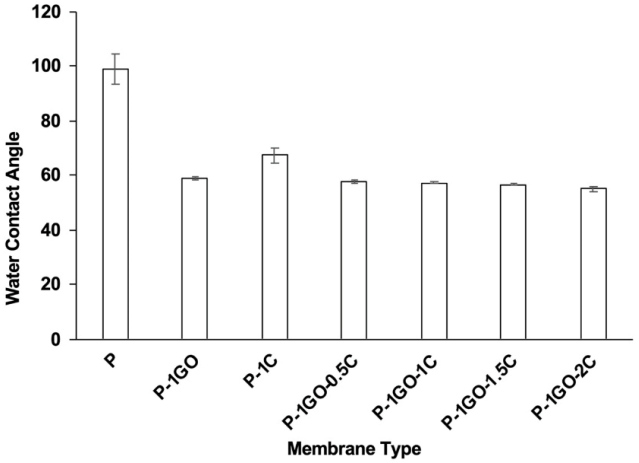

Fig. 5. Contact angles of membranes.

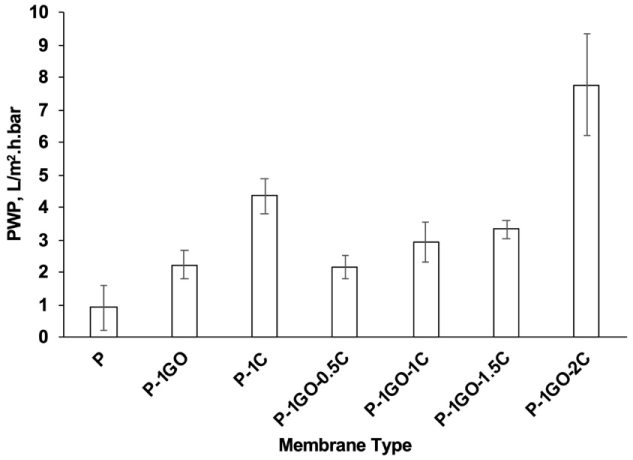

Fig. 6. Pure water permeability of membranes.

compared to the smooth surface of the P-1GO membrane (Fig. 3b) [38]. Thus, the P-1C membrane shows less hydrophilic than the P-1GO membrane. Further improvement of hydrophilicity was observed when CNC and GO filler were combined in the hybrid CNC-GO-PSF membrane, albeit the improvement was not apparent. The membrane hydrophilicity enhancement in the hybrid CNC-GO-PSF membrane is due to abundant hydroxyl groups of the CNC and GO nanoparticles [31]. The increase in membrane hydrophilicity is also contributed by the migration of nanocellulose and GO to the membrane top surface during the phase-inversion process [18,26]. The exposed functional groups accelerate water molecule permeation through membranes [37]. Based on the contact angle result, it can be observed that the amount of GO had a more substantial influence on the hydrophilicity of the hybrid membrane compared to the CNC. The increase in the CNC content of the hybrid CNC-GO-PSF membrane does not significantly affect the contact angle reduction.

3.4. Membrane flux performance

The PWP of membranes is shown in Fig. 6. The range of PWP achieved by the hybrid membrane is comparable to the reported PWP from the literature within the range of 3.47–7.16 L/m²·h·bar [1,37,39]. The PWP increased as the CNC in the hybrid CNC-GO-PSF membrane increased, reaching a maximum value of 7.76 L/m²·h·bar for the membrane P-1GO-2C. The PWP of synthetic membranes is correlated by their porosity, hydrophilicity, and pore diameter [10,40]. The permeability enhancement in the hybrid CNC-GO-PSF membrane was due to the membrane's increased hydrophilicity and porosity, aligning well with the reported contact angle in Fig. 5 and porosity in Fig. 4.

Fig. 7 shows the membrane's water and copper solute flux at 3 bar. The flux of the PSF membrane improved when CNC or GO nanofiller was incorporated into the membrane. The flux for the P-1GO membrane is lower than the P-1C membrane, although the GO membrane had higher porosity and hydrophilicity than the CNC membrane. This low flux can be due to the dense structure of the skin layer of the P-1GO membrane, as shown previously in the SEM

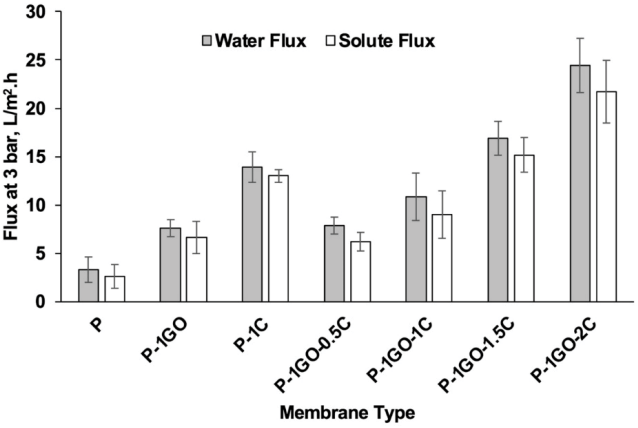

Fig. 7. Pure water and solute flux of membranes.

image of the membrane's top surface. P-1C showed a more porous skin layer compared to the P-1GO membrane. When GO was added to the CNC membrane in the hybrid CNC-GO-PSF membrane, the flux initially dropped but then progressively increased as the CNC content increased. The flux enhancement can be related to the increment of the hybrid membrane porosity and low contact angle compared to a single nanofiller membrane [10,41,42]. The highest water and copper flux was shown by the P-1GO-2C membrane that contained the highest CNC content of 2 wt.%.

3.5. Copper rejection analysis

The copper rejection of the membrane is shown in Fig. 8. The copper rejection of the hybrid membrane had reduced drastically compared to the pristine PSF membrane. The copper rejection of the pristine PSF membrane and P-1GO-2C was around 76% and 27%, respectively. The dispersion of CNC and GO on the membrane solution during the phase inversion process contributes to multiple pores in the hybrid CNC-GO-PSF membrane. The porosity of the hybrid CNC-GO-PSF membrane increased, and the sub-layer structure is becoming very loose, as shown

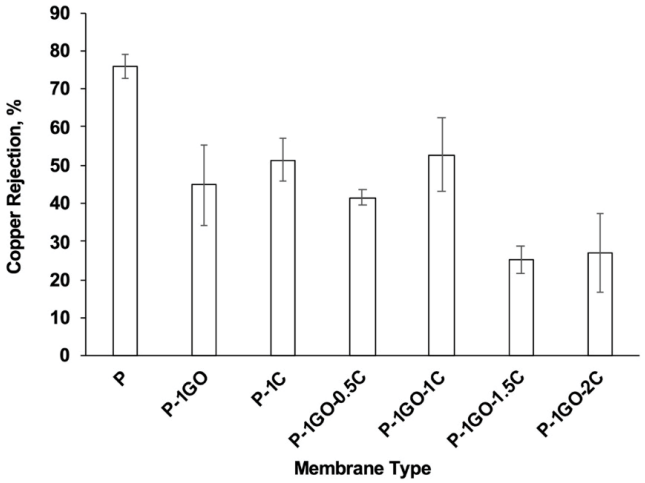

Fig. 8. Copper rejection of membranes.

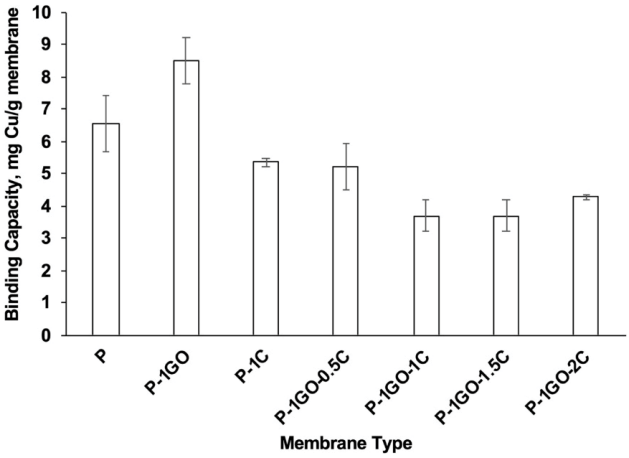

Fig. 9. Binding capacity of membranes.

Table 2
Copper adsorption capacity of various types of membrane

Membrane	Maximum adsorption capacity, $mg \cdot g^{-1}$	Filtration condition	pH	References
HNT/PVDF	0.50	C_i = 5 mg/L TMP = 3 bar	5.5	[37]
PSF/Zeolite	2.82	C_i = 5 mg/L TMP = 0.5 bar	5.0	[43]
PES/Al_2O_3	14.0	C_i = 20 mg/L TMP = 4.5 bar	5	[45]
Regenerated cellulose grafted with P(MA-co-AA)	17.3	C_i = 1 mg/L TMP = 1 bar	6	[44]
PANI/Fe_3O_4/PES	1.6	C_i = 20 mg/L TMP = 4.5 bar	5	[46]
PSF/GO	8.49	C_i = 50 mg/L TMP = 3 bar	6	This study
PSF/CNC/GO	5.30	C_i = 50 mg/L TMP = 3 bar	6	This study

HNT – halloysite nanotubes; PVDF – polyvinylidene fluoride; PES – polyethersulfone; P(MA-co-AA) – poly(maleic anhydride-co-acrylic acid); PANI – polyaniline

in the SEM image previously. As porosity increases, there is less contact between metal ions and surface functional groups, resulting in lower removal percentages [10]. Most modified membranes showed copper rejection below 50%, which could not remove copper effectively. The copper rejection decreased when the amount of CNC increased in the hybrid CNC-GO-PSF membrane. As shown in Fig. 3 previously, the size and number of pores on the top surface of the hybrid membrane increased when more CNC was added. In addition, the porosity of the hybrid membrane was also increased. All these properties reduced the copper rejection as the CNC amount was raised in the hybrid CNC-GO-PSF membrane. Therefore, the feasibility of the modified membrane to operate in the adsorptive filtration mode was investigated and discussed in the following section.

3.6. Copper ion adsorption

The adsorption capacity of the membranes towards copper is shown in Fig. 9. Although the pristine PSF membrane had the highest copper rejection, its binding capacity is lower than the P-1GO membrane. The rejection of the solute in the membrane can be related to several mechanisms, such as sieving and molecular diffusion. At the same time, the binding event can be related to the affinity interaction between the solute and the membrane. Therefore, there is no direct relationship between the rejection and binding capacity value. As no specific active groups or filler are added to the pristine membrane, the binding capacity of the pristine membrane is mainly contributed by the nonspecific binding due to the high hydrophobicity value. The highest copper binding capacity was exhibited by the GO membrane, with

a capacity of 8.49 mg·Cu/g membrane. The oxygen functionalized group in the GO membrane facilitates the adsorption of copper in the P-1GO membrane, thus contributing to high binding capacity. Blending both CNC and GO in the PSF membrane does not improve the copper binding capacity in the hybrid CNC-GO-PSF membrane. Increasing the CNC content in the hybrid CNC-GO-PSF membrane had reduced the copper binding capability of the hybrid membrane. Adding an additional functional group in the membrane shows less influence on the binding capacity. The porosity effect significantly influences the copper binding capacity by reducing the surface contact area of the membrane toward copper ions when the porosity of the hybrid membrane increases. Nevertheless, the binding capacity achieved from this study was comparable with reported membranes as tabulated in Table 2. The PSF/GO membrane had a higher capacity compared to the PSF membrane blend with zeolite [43] or PVDF membrane blended with 3-aminopropyltriethoxysilane functionalized halloysite nanotubes [37]. However, the adsorptive performance of the PSF/GO membrane is still low compared to the recently produced grafted poly(-maleic anhydride-co-acrylic acid) cellulose membrane synthesis through a layer-by-layer method that had a capacity of 17.3 mg copper/g membrane [44].

4. Conclusions

The hybrid PSF UF membranes with GO and CNC were successfully fabricated for copper removal. The porosity, hydrophilicity, and pure water flux of the hybrid membranes were improved by adding CNC and GO as both nanofillers aid in the formation of greater porosity by attracting more water into the membrane matrix during the phase inversion process. Filler addition (GO or CNC or both) in the PSF membrane reduced the copper rejection compared to the pristine PSF membrane due to the unfavorable pore structure and properties. Blending single GO in the PSF membrane enhanced the copper binding capacity of the membrane. Although the current hybrid CNC-GO-PSF membrane showed relatively low rejection for heavy metals, it can be potentially used in other applications, such as humic acid removal from river water. In this application, a hydrophilic membrane is preferable to minimize membrane fouling during filtration [47,48]. In previous studies, a single CNC [49,50] or GO [51,52] based membrane has been successfully used for humic acid removal. Furthermore, as this study kept the GO content in the hybrid membrane constant, there is a possibility that an optimum ratio of GO-CNC in the membrane exists that require further investigation.

Funding

The authors would like to thank the Ministry of Higher Education Malaysia for financial support through the Malaysian Research University Network (MRUN) under the grant code RDU 192302 at Universiti Malaysia Pahang and MRUN-RAKAN RU-2019-004/3 at Universiti Kebangsaan Malaysia. The support received from Universiti Malaysia Pahang through Post Graduate Research Grant – PGRS1903126 was also acknowledged.

Conflict of interest

The authors declare that they have no conflicts of interest.

Credit author statement

Siti Nurul Najiah A. Rasid: Investigation; Nor Azura C. Mahmud: Writing – Original Draft; Syed M. Saufi: Supervision, Conceptualization, Writing – Review & Editing; Mohd Sobri Takriff: Conceptualization; Wei Lun Ang: Writing – Review & Editing.

References

[1] M.T. Hoang, T.D. Pham, D. Verheyen, M.K. Nguyen, T.T. Pham, J. Zhu, B. Van der Bruggen, Fabrication of thin film nanocomposite nanofiltration membrane incorporated with cellulose nanocrystals for removal of Cu(II) and Pb(II), Chem. Eng. Sci., 228 (2020) 115998, doi: 10.1016/j.ces.2020.115998.
[2] W. Liu, D. Wang, R.A. Soomro, F. Fu, N. Qiao, Y. Yu, R. Wang, B. Xu, Ceramic supported attapulgite-graphene oxide composite membrane for efficient removal of heavy metal contamination, J. Membr. Sci., 591 (2019) 117323, doi: 10.1016/j.memsci.2019.117323.
[3] A. Modi, J. Bellare, Zeolitic imidazolate framework-67/carboxylated graphene oxide nanosheets incorporated polyethersulfone hollow fiber membranes for removal of toxic heavy metals from contaminated water, Sep. Purif. Technol., 249 (2020) 117160, doi: 10.1016/j.seppur.2020.117160.
[4] S. Abd Hamid, M. Shahadat, B. Ballinger, S. Farhan Azha, S. Ismail, S. Wazed Ali, S. Ziauddin Ahammad, Role of clay-based membrane for removal of copper from aqueous solution, J. Saudi Chem. Soc., 24 (2020) 785–798.
[5] K.C. Khulbe, T. Matsuura, Removal of heavy metals and pollutants by membrane adsorption techniques, Appl. Water Sci., 8 (2018) 19, doi: 10.1007/s13201-018-0661-6.
[6] M. Hezarjaribi, Gh. Bakeri, M. Sillanpää, M.J. Chaichi, S. Akbari, Novel adsorptive membrane through embedding thiol-functionalized hydrous manganese oxide into PVC electrospun nanofiber for dynamic removal of Cu(II) and Ni(II) ions from aqueous solution, J. Water Process Eng., 37 (2020) 101401, doi: 10.1016/j.jwpe.2020.101401.
[7] A. Ashori, F. Rafieyan, F. Kian, M. Jonoobi, K. Rezaei Tavabe, Effect of cellulose nanocrystals on performance of polyethersulfone nanocomposite membranes using electrospinning technique, Polym. Compos., Special Issue: Structure, Morphology, and Surface Modification, 40 (2019) E835–E841, doi: 10.1002/pc.25046.
[8] M. Jonoobi, A. Ashori, V. Siracusa, Characterization and properties of polyethersulfone/modified cellulose nanocrystals nanocomposite membranes, Polym. Test., 76 (2019) 333–339.
[9] S.A. Hamid, S. Ismail, Effect of sodium dodecyl sulfate (SDS) on polysulfone/zeolite membrane for the removal of copper ions, IOP Conf. Ser.: Mater. Sci. Eng., The 9th AIC 2019 on Sciences & Engineering (9thAIC-SE) 18–20 September 2019, Banda Aceh, Indonesia, 796 (2020) 012053.
[10] S. Mondal, S. Kumar Majumder, Fabrication of the polysulfone-based composite ultrafiltration membranes for the adsorptive removal of heavy metal ions from their contaminated aqueous solutions, Chem. Eng. J., 401 (2020) 126036, doi: 10.1016/j.cej.2020.126036.
[11] P. Moradihamedani, A.H. Abdullah, High-performance cellulose acetate/polysulfone blend ultrafiltration membranes for removal of heavy metals from water, Water Sci. Technol., 75 (2017) 2422–2433.

[12] K.P.Y. Shak, Y.L. Pang, S.K. Mah, Nanocellulose: recent advances and its prospects in environmental remediation, Beilstein J. Nanotechnol., 9 (2018) 2479–2498.
[13] L. Chen, H. Yu, C. Deutschman, T. Yang, K.C. Tam, Novel design of Fe-Cu alloy coated cellulose nanocrystals with strong antibacterial ability and efficient Pb^{2+} removal, Carbohydr. Polym., 234 (2020) 115889, doi: 10.1016/j.carbpol.2020.115889.
[14] W. Li, B. Ju, S. Zhang, A green L-cysteine modified cellulose nanocrystals biosorbent for adsorption of mercury ions from aqueous solutions, RSC Adv., 9 (2019) 6986–6994.
[15] W.-Q. Xie, K.-X. Yu, Y.-X. Gong, Preparation of fluorescent and antibacterial nanocomposite films based on cellulose nanocrystals/ZnS quantum dots/polyvinyl alcohol, Cellulose, 26 (2019) 2363–2373.
[16] P. Lu, Y.-L. Hsieh, Preparation and characterization of cellulose nanocrystals from rice straw, Carbohydr. Polym., 87 (2012) 564–573.
[17] N. Grishkewich, N. Mohammed, J. Tang, K.C. Tam, Recent advances in the application of cellulose nanocrystals, Curr. Opin. Colloid Interface Sci., 29 (2017) 32–45.
[18] F. Rafieian, M. Jonoobi, Q. Yu, A novel nanocomposite membrane containing modified cellulose nanocrystals for copper ion removal and dye adsorption from water, Cellulose, 26 (2019) 3359–3373.
[19] C.H. Park, S. Jeon, S.-H. Park, M.G. Shin, M.S. Park, S.-Y. Lee, J.-H. Lee, Cellulose nanocrystal-assembled reverse osmosis membranes with high rejection performance and excellent antifouling, J. Mater. Chem. A, 7 (2019) 3992–4001.
[20] X. Yang, H. Liu, Y. Zhao, L. Liu, Preparation and characterization of polysulfone membrane incorporating cellulose nanocrystals extracted from corn husks, Fibers Polym., 17 (2016) 1820–1828.
[21] C. Xu, W. Chen, H. Gao, X. Xie, Y. Chen, Cellulose nanocrystal/silver (CNC/Ag) thin-film nanocomposite nanofiltration membranes with multifunctional properties, Environ. Sci.: Nano, 7 (2020) 803–816.
[22] E.S. Snow, F.K. Perkins, E.J. Houser, S.C. Badescu, T.L. Reinecke, Chemical detection with a single-walled carbon nanotube capacitor, Science, 307 (2005) 1942–1945.
[23] J. Ma, D. Ping, X. Dong, Recent developments of graphene oxide-based membranes: a review, Membranes (Basel), 7 (2017) 52, doi: 10.3390/membranes7030052.
[24] H. Huang, Y. Mao, Y. Ying, Y. Liu, L. Sun, X. Peng, Salt concentration, pH and pressure controlled separation of small molecules through lamellar graphene oxide membranes, Chem. Commun., 49 (2013) 5963–5965.
[25] T. Szabó, A. Szeri, I. Dékány, Composite graphitic nanolayers prepared by self-assembly between finely dispersed graphite oxide and a cationic polymer, Carbon, 43 (2005) 87–94.
[26] B.M. Ganesh, A.M. Isloor, A.F. Ismail, Enhanced hydrophilicity and salt rejection study of graphene oxide-polysulfone mixed matrix membrane, Desalination, 313 (2013) 199–207.
[27] H. Ravishankar, J. Christy, V. Jegatheesan, Graphene oxide (GO)-blended polysulfone (PSf) ultrafiltration membranes for lead ion rejection, Membranes (Basel), 8 (2018) 77, doi: 10.3390/membranes8030077.
[28] Z. Wang, H. Yu, J. Xia, F. Zhang, F. Li, Y. Xia, Y. Li, Novel GO-blended PVDF ultrafiltration membranes, Desalination, 299 (2012) 50–54.
[29] R. Mukherjee, P. Bhunia, S. De, Impact of graphene oxide on removal of heavy metals using mixed matrix membrane, Chem. Eng. J., 292 (2016) 284–297.
[30] G. Zhang, J. Lv, F. Yang, Optimized anti-biofouling performance of bactericides/cellulose nanocrystals composites modified PVDF ultrafiltration membrane for micro-polluted source water purification, Water Sci. Technol., 79 (2019) 1437–1446.
[31] P. Daraei, N. Ghaemi, H. Sadeghi Ghari, An ultra-antifouling polyethersulfone membrane embedded with cellulose nanocrystals for improved dye and salt removal from water, Cellulose, 24 (2017) 915–929.
[32] N.D. Koromilas, C. Anastasopoulos, E.K. Oikonomou, J.K. Kallitsis, Preparation of porous polymeric membranes based on a pyridine containing aromatic polyether sulfone, Polymers (Basel), 11 (2019) 59, doi: 10.3390/polym11010059.
[33] A. Alkhouzaam, H. Qiblawey, Novel polysulfone ultrafiltration membranes incorporating polydopamine functionalized graphene oxide with enhanced flux and fouling resistance, J. Membr. Sci., 620 (2021) 118900, doi: 10.1016/j.memsci.2020.118900.
[34] S. Zinadini, A.A. Zinatizadeh, M. Rahimi, V. Vatanpour, H. Zangeneh, Preparation of a novel antifouling mixed matrix PES membrane by embedding graphene oxide nanoplates, J. Membr. Sci., 453 (2014) 292–301.
[35] J. Lv, G. Zhang, H. Zhang, F. Yang, Graphene oxide-cellulose nanocrystal (GO-CNC) composite functionalized PVDF membrane with improved antifouling performance in MBR: behavior and mechanism, Chem. Eng. J., 352 (2018) 765–773.
[36] N.F.D. Junaidi, N.A. Khalil, A.F. Jahari, N.Z.K. Shaari, M.Z. Shahruddin, N.H. Alias, N.H. Othman, Effect of graphene oxide (GO) on the surface morphology & hydrophilicity of polyethersulfone (PES), IOP Conf. Ser.: Mater. Sci. Eng., 3rd International Conference on Global Sustainability and Chemical Engineering (ICGSCE) 15–16 February 2017, Putrajaya, Malaysia, 358 (2018) 012047.
[37] G. Zeng, Y. He, Y. Zhan, L. Zhang, Y. Pan, C. Zhang, Z. Yu, Novel polyvinylidene fluoride nanofiltration membrane blended with functionalized halloysite nanotubes for dye and heavy metal ions removal, J. Hazard. Mater., 317 (2016) 60–72.
[38] Y.H. Teow, B.S. Ooi, A.L. Ahmad, Fouling behaviours of PVDF-TiO_2 mixed-matrix membrane applied to humic acid treatment, J. Water Process Eng., 15 (2017) 89–98.
[39] G. Abdi, A. Alizadeh, S. Zinadini, G. Moradi, Removal of dye and heavy metal ion using a novel synthetic polyethersulfone nanofiltration membrane modified by magnetic graphene oxide/metformin hybrid, J. Membr. Sci., 552 (2018) 326–335.
[40] C. Lavanya, R.G. Balakrishna, K. Soontarapa, M.S. Padaki, Fouling resistant functional blend membrane for removal of organic matter and heavy metal ions, J. Environ. Manage., 232 (2019) 372–381.
[41] W. Fu, L. Hua, W. Zhang, Experimental and modeling assessment of the roles of hydrophobicity and zeta potential in chemically modified poly(ether sulfone) membrane fouling kinetics, Ind. Eng. Chem. Res., 56 (2017) 8580–8589.
[42] D. Han, L. Yan, W. Chen, W. Li, P.R. Bangal, Cellulose/graphite oxide composite films with improved mechanical properties over a wide range of temperature, Carbohydr. Polym., 83 (2011) 966–972.
[43] S.A. Hamid, S.F. Azha, L. Sellaoui, A. Bonilla-Petriciolet, S. Ismail, Adsorption of copper (II) cation on polysulfone/zeolite blend sheet membrane: synthesis, characterization, experiments and adsorption modelling, Colloids Surf., A, 601 (2020) 124980, doi: 10.1016/j.colsurfa.2020.124980.
[44] X. Pei, L. Gan, Z. Tong, H. Gao, S. Meng, W. Zhang, P. Wang, Y. Chen, Robust cellulose-based composite adsorption membrane for heavy metal removal, J. Hazard. Mater., 406 (2021) 124746, doi: 10.1016/j.jhazmat.2020.124746.
[45] N. Ghaemi, A new approach to copper ion removal from water by polymeric nanocomposite membrane embedded with γ-alumina nanoparticles, Appl. Surf. Sci., 364 (2016) 221–228.
[46] P. Daraei, S.S. Madaeni, N. Ghaemi, E. Salehi, M.A. Khadivi, R. Moradian, B. Astinchap, Novel polyethersulfone nanocomposite membrane prepared by PANI/Fe_3O_4 nanoparticles with enhanced performance for Cu(II) removal from water, J. Membr. Sci., 415–416 (2012) 250–259.
[47] A. Mautner, Nanocellulose water treatment membranes and filters: a review, Polym. Int., This Article Also Appears in: United Nations' Sustainable Development Goals: Research on Access to Justice, 69 (2020) 741–751.
[48] R. Reshmy, D. Thomas, E. Philip, S.A. Paul, A. Madhavan, R. Sindhu, P. Binod, A. Pugazhendhi, R. Sirohi, A. Tarafdar, A. Pandey, Potential of nanocellulose for wastewater treatment, Chemosphere, 281 (2021) 130738, doi: 10.1016/j.chemosphere.2021.130738.
[49] H. Sehaqui, B. Michen, E. Marty, L. Schaufelberger, T. Zimmermann, Functional cellulose nanofiber filters with

enhanced flux for the removal of humic acid by adsorption, ACS Sustainable Chem. Eng., 4 (2016) 4582–4590.
[50] E. Pramono, M.A. Zakaria, K.F. Fridiasari, S.T.C.L. Ndruru, M. Bagaskara, R.E. Mustofa, G.P.W. Sejati, C. Purnawan, O.A. Saputra, Cellulose derived from oil palm empty fruit bunches as filler on polyvinylidene fluoride based membrane for water containing humic acid treatment, Groundwater Sustainable Dev., 17 (2022) 100744, doi: 10.1016/j.gsd.2022.100744.
[51] J.J. Song, Y. Huang, S.-W. Nam, M. Yu, J. Heo, N. Her, J.R.V. Flora, Y. Yoon, Ultrathin graphene oxide membranes for the removal of humic acid, Sep. Purif. Technol., 144 (2015) 162–167.
[52] M.S. Algamdi, I.H. Alsohaimi, J. Lawler, H.M. Ali, A.M. Aldawsari, H.M.A. Hassan, Fabrication of graphene oxide incorporated polyethersulfone hybrid ultrafiltration membranes for humic acid removal, Sep. Purif. Technol., 223 (2019) 17–23.